Hindawi Publishing Corporation
Advances in Materials Science and Engineering
Volume 2015, Article ID 564876, 11 pages
http://dx.doi.org/10.1155/2015/564876

Research Article

Shear Strengthening Performance of Hybrid FRP-FRCM

Kyusan Jung, Kinam Hong, Sanghoon Han, Jaekyu Park, and Jaehyun Kim

Department of Civil Engineering, Chungbuk National University, 1 Chungdae-Ro, Seowon-Gu, Cheongju, Chungbuk 362-763, Republic of Korea

Correspondence should be addressed to Kinam Hong; hong@cbnu.ac.kr

Received 28 April 2015; Accepted 8 June 2015

Academic Editor: Ana S. Guimarães

The effectiveness of a hybrid fiber reinforced polymer- (FRP-) fabric reinforced cementitious matrix (FRCM) for shear strengthening was investigated though an experimental study. FRP materials of FRCM are usually fabricated in the form of a fabric to enhance the bond strength between the FRP material and the cementitious matrix. The hybrid FRP fabric used in this study consisted of carbon FRP (CFRP) and glass FRP (GFRP) in warp and weft directions, respectively. A total of 11 beams were fabricated and 8 beams among them were strengthened in shear with externally bonded hybrid FRP-FRCM. The number of plies, the bond types, and the spacing of the hybrid FRP fabric were considered as experimental variables. Additionally, a shear capacity model for a FRCM shear strengthened beam was proposed. The values predicted by the proposed model were compared with those by the ACI 549 code and test results. It was confirmed from the comparison that the proposed model predicted the shear strengthening performance of the hybrid FRP-FRCM more reliably than the ACI 549 code did.

1. Introduction

FRP has been widely used as a strengthening material to strengthen deteriorated reinforced concrete (RC) structures all over the world [1]. As a strengthening material, FRP possesses excellent material properties including being lightweight and noncorrosive and providing high tensile strength [2]. On this basis, FRP has been applied for strengthening RC structures in various forms such as sheets, plates, and strips since the early 1990s [3]. Many studies on FRP have validated the effectiveness of its use as a strengthening material [4]. However, FRP is accompanied by several distinct disadvantages. The performance of FRP strengthening for RC structures, which may be exposed to sunlight or high temperature conditions, is degraded due to the low glass transition temperature of epoxy resin, a bonding agent. FRP strengthening using epoxy resin is also vulnerable to fire. Additionally, epoxy resin cannot be used under a wet condition due to its low hardening property.

In order to solve these problems, a strengthening method using a fabric-reinforced cementitious matrix (FRCM) was developed [5]. FRCM consists of FRP fabric and a cementitious matrix. The mineral cementitious matrix can solve various problems caused by using epoxy resin as a bonding agent. FRCM was first introduced as textile reinforced concrete (TRC) in a report published by RILEM Technical Committee 201 [6]. It has since then been widely reported on in the literature with various names including textile reinforced mortar (TRM) [7], fiber reinforced concrete (FRC) [8], and mineral based composites (MBC) [9].

Research using FRCM as a shear strengthening material has been performed by researchers worldwide. Baggio et al. performed experimental research on RC beams strengthened in shear with CFRP, GFRP, FRCM, and FRP anchors [10]. The effectiveness of each material in terms of shear strengthening was evaluated and test results were compared with predicted values by the Canadian design code. Beams strengthened by using FRCM with and without anchors showed a 31% and 34% increase in shear capacity relative to the Control specimen, respectively. The Canadian design code appropriately predicted the shear capacity of beams strengthened with FRP sheets but overestimated those of FRCM strengthened beams. Triantafillou and Papanicolaou carried out an experimental study to investigate the effectiveness of CFRP-FRCM shear strengthening [7]. Although the effectiveness of FRCM shear strengthening was relatively lower than FRP

shear strengthening, the applicability of FRCM as a shear strengthening material was validated. Ombres experimentally examined the effectiveness of polyparaphenylene benzobisoxazole (PBO) FRCM for shear strengthening [11]. Its shear strengthening performance was predicted by a model based on Ritter-Morsch criteria failure. He reported that the PBO-FRCM strengthening system significantly improved the shear capacity of reinforced concrete beams and prediction by the model based on the Ritter-Morsch criteria failure is effective to predict the PBO-FRCM performance. Brückner et al. experimentally explored the effectiveness of GFRP-FRCM for shear strengthening [12, 13]. The number of GFRP plies, the use of mechanical anchors, and anchorage methods were considered as experimental variables in their study. Their test results showed that FRCM is effective for shear strengthening and the mechanical anchor improves the FRCM shear strengthening performance by 200%. Al-Salloum et al. also reported that FRCM is effective in increasing the shear capacity of beams subjected to a four-point load [14]. Recently, a design code for strengthening RC structures and masonry walls with externally bonded FRCM was issued by ACI Committee 549 [15].

Nevertheless, the applicability of existing design codes should be established by experimentally exploring the influence of various experimental parameters such as concrete strength, cementitious matrix type, and FRP material type on shear strengthening. Experimental research on RC beams strengthened in shear with externally bonded FRCM, which was made from a hybrid fabric and a cementitious matrix, was performed in this study. The number of plies, the bond type, and the spacing of a hybrid FRP fabric were considered as experimental variables. The effect of test variables on the shear strengthening capacity was evaluated through test results and a shear strength prediction model for a hybrid FRP-FRCM strengthened beam was proposed. The values predicted by the proposed model were compared with those by ACI 549 [15] and test results.

2. Test Program

2.1. Used Materials. Type I ordinary Portland cement (OPC) was used in the mixture. Crushed gravel was used as the coarse aggregate and the maximum aggregate size was 25 mm. In addition, AE water-reducing admixture and a vibrator were used to improve the workability and consolidation of the concrete. Table 1 shows the mixture properties of the used concrete.

Concrete compressive strength was determined from a compression test for six cylinders with dimensions of ø100 mm × 200 mm according to ASTM C39/C39M [18]. The average concrete compressive strength was 28.0 MPa at the age of 28 days. The mechanical properties of each used rebar were determined from tension tests for three coupons according to ASTM A370 [19] and the results are given in Table 2.

The cementitious matrix and the hybrid FRP fabric used for shear strengthening of RC specimens in this study are shown in Figures 1(a) and 1(b), respectively. Cementitious matrix consisted of microcement, fine aggregate, polypropylene staple fiber, and admixtures. The compressive strength of the cementitious matrix was determined from a compression test for five cubes of 50 mm size according to ASTM C109/C109M [20] and taken as 45 MPa at the age of 28 days. As shown in Figure 1(b), the hybrid FRP fabric consisted of CFRP and GFRP strips. Black CFRP and white GFRP strips were laid in the warp direction and weft direction, respectively, at spacing of 17 mm and 33 mm. Mechanical properties of the FRCM composite made from the hybrid FRP fabric and the cementitious matrix were determined by a direct tensile test in accordance with AC 434 [16], as shown in Figure 2. Table 3 presents the mechanical properties of the hybrid FRP fabric and the cementitious matrix offered by manufacturers and those of the FRCM composite obtained from the direct tensile test.

Table 1: Mixture properties of the concrete.

W/C (%)	S/a (%)	Unit weight (kg/m^3)				
		W	C	S	G	Ad[(a)]
48.4	48.1	168	345	860	949	2.07

[(a)] AE water-reducing admixture.

2.2. Test Variables. As shown in Table 4, specimens were classified into four groups. Specimens in Group I consisted of nonstrengthened specimen and steel stirrup-strengthened specimens to evaluate the relative shear-strengthening performance of the hybrid FRP-FRCM.

The nonstrengthened specimen was designated as Control, and the specimens reinforced with steel stirrups at spacing of 200 mm and 300 mm were denoted by S200 and S300, respectively. Specimens in Group II consisted of specimens strengthened in shear by side-bonding. The specimens were named according to the width and the number of plies of the used hybrid FRP fabric. The specimens strengthened with 1-ply and 2-ply 600 mm hybrid FRP fabric were designated as W600-L1 and W600-L2, respectively. Specimens in Groups III and IV consisted of specimens strengthened by U-jacketing. The specimens strengthened by U-jacketing were named according to the width and number of plies of hybrid FRP fabric. For example, W50-N5 was strengthened with 5 pieces of 50 mm wide hybrid FRP fabric. The sixth column of Table 4 shows hybrid FRP fabric attached on the shear span according to experimental variables.

2.3. Specimen Fabrication and Strengthening. As shown in Figure 3, a total of 11 specimens having a length of 2,000 mm with a rectangular cross-section 150 mm wide and 300 mm high and a net span of 1,800 mm were fabricated for the tests. All specimens were reinforced with two rebars with a nominal diameter of 15.9 mm as tension reinforcement and two rebars with a nominal diameter of 9.53 mm as compression reinforcement.

Specimens S200 and S300 were reinforced by rebars with a nominal diameter of 9.53 mm with spacing of 200 mm and 300 mm as shear reinforcement, respectively. After curing of 28 days, the shear strengthening specimens were strengthened with the hybrid FRP-FRCM as follows. First, the specimen surface was cleaned with tap water to remove

(a) Cementitious matrix (b) Hybrid FRP fabric

Figure 1: Components of hybrid FRP-FRCM system.

(a) Test setup for direct tensile testing of a flat hybrid FRP-FRCM coupon

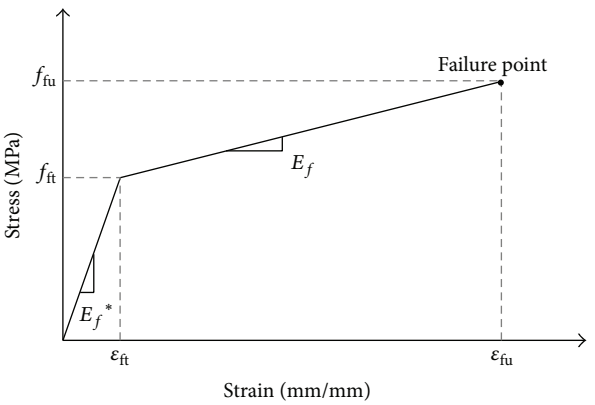

(b) Idealized tensile stress-strain curve for FRCM

Figure 2: Direct tensile testing by AC 434 [16].

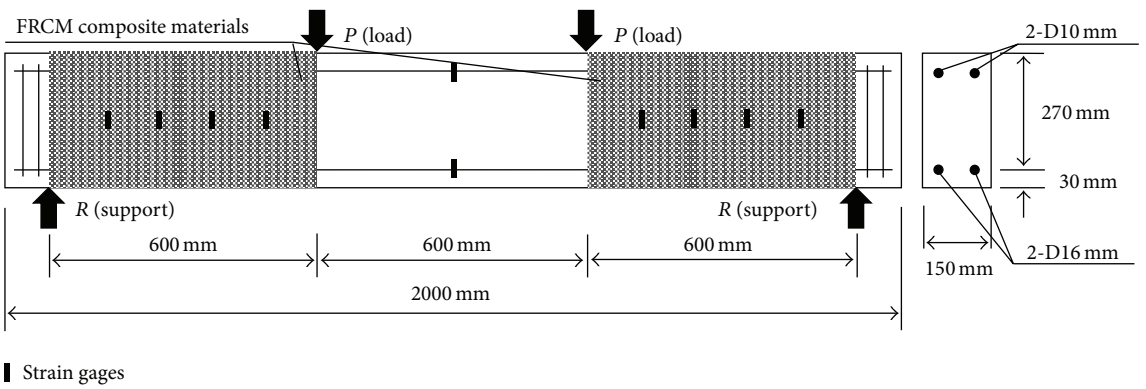

Figure 3: Test specimen layout.

Table 2: Mechanical properties of rebar.

Nominal diameter (mm)	Modulus of elasticity (MPa)	Yield strength (MPa)	Tensile strength (MPa)	Elongation (%)
9.53	2.0×10^5	480	590	17.1
15.9		515	610	16.6

Table 3: Hybrid FRP-FRCM mechanical properties.

	Nominal thickness (mm)	Elastic modulus (GPa)	Ultimate tensile strength (MPa)	Ultimate tensile strain (%)	Compression strength (MPa)
Hybrid fabric	0.107	240	4,300	1.75	—
Cementitious matrix	—	40	—	—	45
FRCM composite	—	160 (cracked specimen)	800	0.5	—

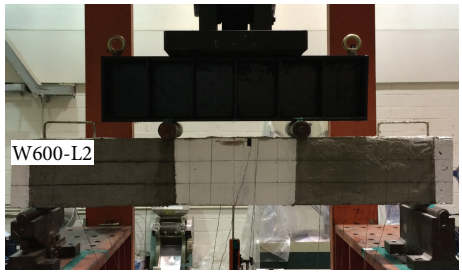

Figure 4: Test setup.

impurities before strengthening. In order to keep the humid condition, the specimen surface was then covered with damp cloth until strengthening work. Specimens strengthened by U-jacketing were reversed and then chamfered to a radius of 10 mm to avoid damage to the hybrid FRP fabric due to stress concentration during the tests. Specimens were strengthened with hybrid FRP-FRCM according to the test variables. The strengthening procedure of the FRCM composite was as follows: (1) the first layer of cementitious matrix with a nominal thickness of 2 mm was applied on the side surface of the specimen; (2) the precut hybrid FRP fabric was laid on the cementitious matrix; and (3) the second layer of cementitious matrix with a nominal thickness of 2 mm was applied on the hybrid FRP fabric. In the case of strengthening with 2-ply hybrid FRP fabric, the above procedure was repeated two times. The nominal thickness of hybrid FRP-FRCM with 1-ply hybrid FRP fabric was taken as approximately 5 mm. Tests were performed after 28 days of strengthening for the cementitious matrix to develop sufficient strength.

2.4. Test Setup. The shear tests for 11 specimens were performed by four-point loading, as shown in Figure 4. The specimens were simply supported and the load was applied at two points 300 mm apart at both the left and right sides of the midspan. The load was applied by stroke control loading at a rate of 0.4 mm/min with a hydraulic actuator with a maximum capacity of 2,000 kN. The load was measured by a load cell. The vertical displacement at the midspan was measured by two linear variable differential transformers (LVDTs).

As shown in Figure 3, the strain of the hybrid FRP fabric was measured by eight strain gauges attached on the CFRP fabric strips at both the left and right sides of the shear span. The CFRP strip of the hybrid FRP fabric was grinded and cleaned with acetone before attachment of strain gauges. Load and strains were recorded by using a data logger. Crack propagation and FRCM composite damage were visually monitored and recorded during all tests.

3. Test Results and Discussion

3.1. Shear Resisting Capacity. The test results, the maximum load, the displacement corresponding to the maximum load, the gain of the maximum load, and the failure mode are presented in Table 5.

The specimen Control failed due to a diagonal shear crack at the maximum load of 105 kN (see Figure 5(a)), while specimens S200 and S300 strengthened with steel stirrup failed due to the yielding of the tensile steel followed by the crushing of concrete at maximum load of 168 kN and 172 kN, respectively (see Figure 5(b)). Specimens W600-L1 and W600-L2 strengthened by side-bonding failed due to debonding of the FRCM composite at maximum load of 132 kN and 152 kN, respectively (see Figure 5(c)). The maximum loads of specimens W600-L1 and W600-L2 increased by 36.2% and 44.8%, respectively, when compared with the Control specimen. Although the maximum load increased with an increasing number of plies of hybrid fabric, it did not increase in proportion to the amount of the hybrid fabric.

Specimens in Group III failed due to debonding of the FRCM composite at the maximum load from 117 kN to 127 kN according to the amount of hybrid FRP fabric. The maximum loads of specimens W50-N4, W50-N5, and W50-N6 increased by 11.4%, 17.1%, and 21.0% relative to the unstrengthened specimen, respectively. The maximum loads of specimens W100-N3 and W100-N4 in Group IV were 121 kN and 144 kN, respectively, and their strength increased by 15.2% and 37.1% relative to the unstrengthened specimen,

Table 4: Test variables.

Group	Specimen ID	Strengthening type	Layer	Width × number	Installation
I	Control	None	None	None	None
	S300	Steel stirrup	None	None	None
	S200				
II	W600-L1	Side-bonding	1	600 mm × 1	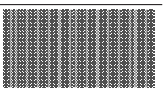
	W600-L2		2		
III	W50-N4	U-jacketing	1	50 mm × 4	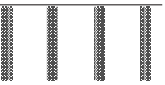
	W50-N5			50 mm × 5	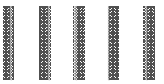
	W50-N6			50 mm × 6	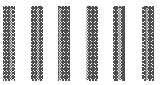
	W100-N3			100 mm × 3	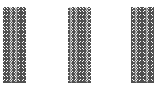
IV	W100-N4			100 mm × 4	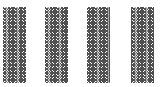
	W600-N1			600 mm × 1	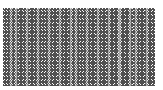

Table 5: Summary of test results.

Specimen ID	Maximum load (kN)	Displacement corresponding to maximum load (mm)	Gain of maximum load (%)	Failure mode
Control	105	7.2	—	Shear
S300	172	20.2	63.8	Flexure
S200	168	19.2	60.0	
W600-L1	143	8.3	36.2	Debonding
W600-L2	152	10.2	44.8	
W50-N4	117	6.7	11.4	
W50-N5	123	5.3	17.1	
W50-N6	127	7.4	21.0	
W100-N3	121	6.2	15.2	
W100-N4	144	8.6	37.1	
W600-N1	162	9.2	54.3	

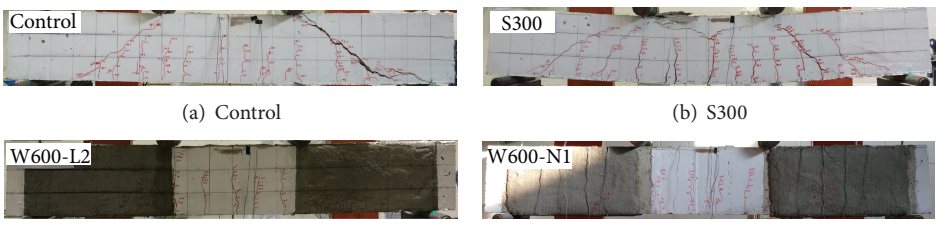

(a) Control (b) S300

(c) W600-L2 (d) W600-N1

Figure 5: Specimens after test.

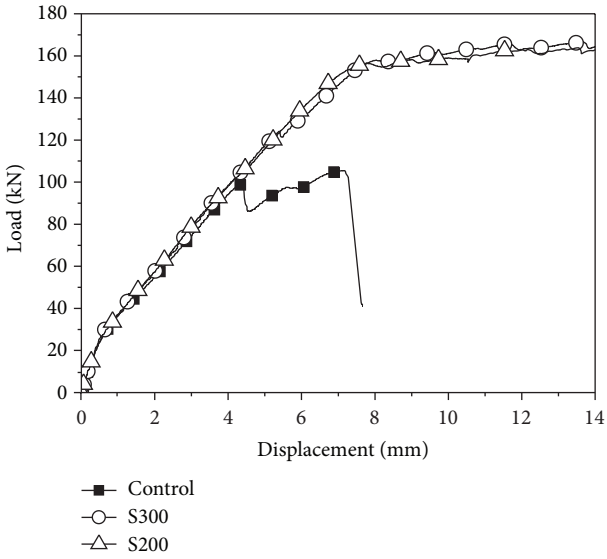

Figure 6: Load-displacement curves of specimens in Group I.

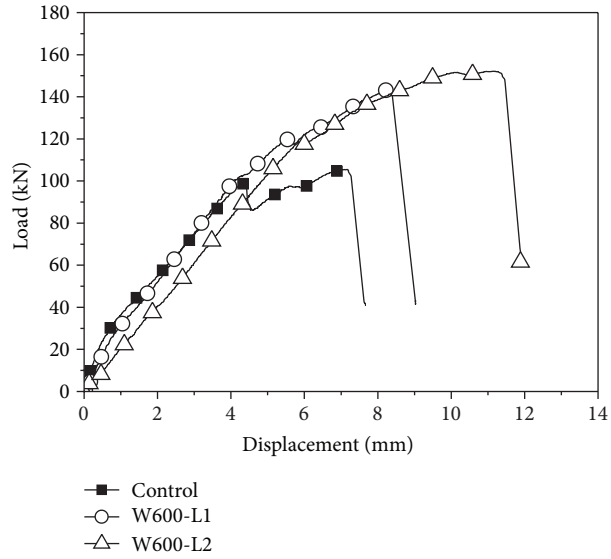

Figure 7: Load-displacement curves of specimens in Group II.

respectively. All specimens in Group IV failed due to debonding of the FRCM composite, similar to specimens in Group III. The maximum load of specimen W600-N1 was 162 kN and increased by 54.3% relative to the Control specimen (see Figure 5(d)). The difference in the maximum load of specimens W50-N6 and W100-N3 with the same amount of hybrid FRP fabric was about 6 kN. This resulted from the difference in the spacing of the hybrid FRP with specimens W50-N6 and W100-N3. The difference in the maximum loads of W600-L1 and W600-N1 with the same amount of hybrid FRP fabric was 30 kN. It can be confirmed from this result that U-jacketing is more effective than side-bonding.

3.2. Load-Displacement Relationship. The load-displacement curves of specimens in Group I are presented in Figure 6.

For the specimen Control, the load started to decrease with the occurrence of diagonal shear cracks at displacement of 4.4 mm and it failed due to a shear crack at displacement of 7.2 mm. For specimens S200 and S300 reinforced with steel stirrups, the maximum load increased over that of specimen Control and they failed due to the yielding of tensile reinforcement followed by the crushing of concrete. The load-displacement curves of specimens in Group II are shown in Figure 7. This figure shows that specimen W600-L2 has higher shear capacity and ductility than specimen W600-L1. The load-displacement curves of specimens in Group III are presented in Figure 8.

Figure 8 shows that although the load-displacement curve of specimen W50-N5 is different from those of W50-N4 and W50-N6, the shear capacity increases with a higher amount of hybrid FRP fabric. The load-displacement curves of specimens in Group IV are presented in Figure 9. The load of specimen W100-N3 started to decrease at a displacement of 6.2 mm and it failed due to debonding of the FRCM composite at a displacement of 8.4 mm. For specimens W100-N4 and W600-N1, although their stiffness decreased at a displacement of 5 mm, at which a shear crack of specimen

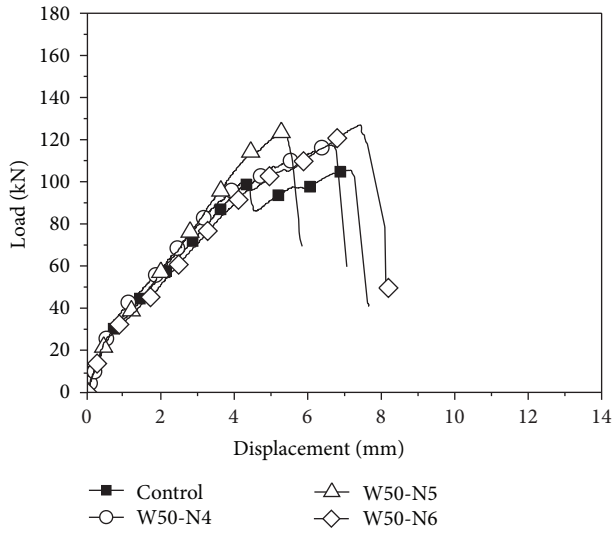

Figure 8: Load-displacement curves of specimens in Group III.

Control occurred, the load continued to increase. In particular, the maximum load of specimen W600-N1 was similar to that of specimen S300. Therefore, it can be confirmed that U-jacketing is more effective for FRCM shear strengthening, and hybrid FRP-FRCM is applicable for shear strengthening of RC beams.

3.3. Strain of Hybrid FRP Fabric. Strains of hybrid FRP fabric obtained from specimens W600-L1 and W600-L2 are, respectively, presented in Figure 10. The strains were measured from strain gauges on the hybrid FRP fabric installed at the center of the shear span. The hybrid FRP fabric strain of specimens W600-L1 and W600-L2 did not increase before the initial shear crack occurred. The strain of W600-L1 started to move after the initial diagonal shear crack and increased sharply after a load of 80 kN, at which the shear crack was completely

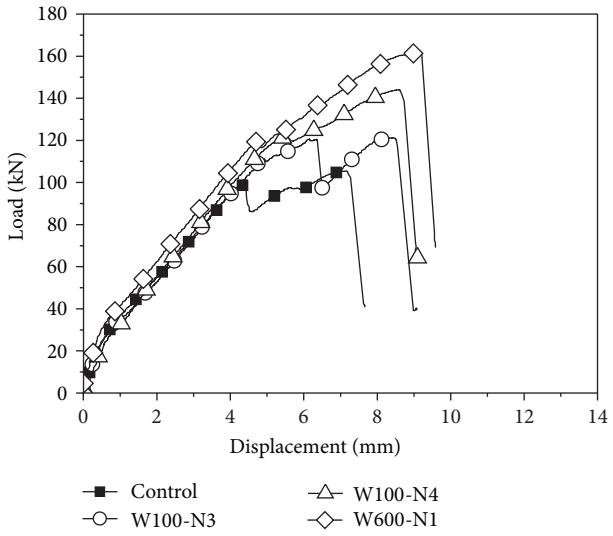

Figure 9: Load-displacement curves of specimens in Group IV.

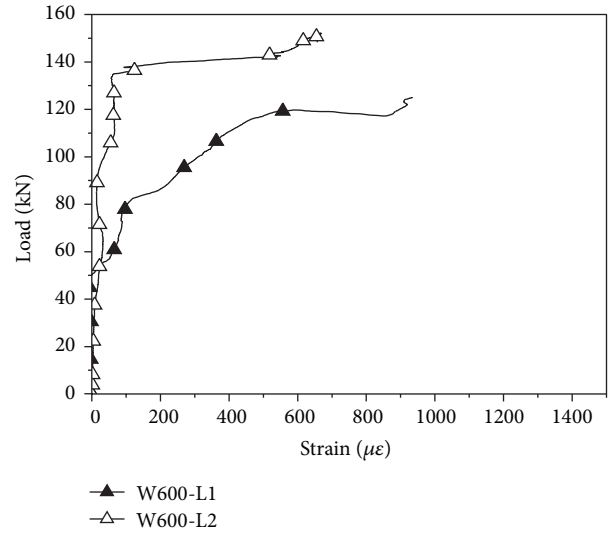

Figure 10: Load-strain curves of hybrid FRP-FRCM system.

formed. The strain of specimen W600-L2 with 2 plies of hybrid FRP fabric started to increase at a higher load than specimen W600-L1 with 1 ply of hybrid FRP fabric. The maximum strains of the hybrid FRP fabric of these specimens were much smaller than 0.0175, the strain corresponding to rupture of the CFRP fabric strip. This result indicates that the failure of the specimen strengthened in shear with the hybrid FRP-FRCM composite is not due to rupture of the hybrid FRP fabric but rather due to debonding between concrete and the FRCM composite.

3.4. Prediction of Shear Capacity

3.4.1. ACI Code. In order to predict the shear capacity of beams strengthened with FRCM, ACI Committee 549 [15] has proposed the following equation:

$$V_n = V_c + V_s + V_f, \tag{1}$$

where V_n is the nominal shear strength and V_c, V_s, and V_f are the contribution of concrete, existing steel reinforcement, and FRCM composite material to the nominal shear strength, respectively.

The contribution of concrete and steel reinforcement to the nominal shear strength is calculated according to the following equation proposed by ACI 318 [21]:

$$\begin{aligned} V_c &= 0.17\sqrt{f_c'}\, b_w d, \\ V_s &= \frac{A_v f_{\mathrm{yt}} d}{s}, \end{aligned} \tag{2}$$

where f_c' is the specified compressive strength of concrete; b_w is the web width and d is the distance from the extreme compression fiber to the centroid of longitudinal tension reinforcement; A_v is the area of shear reinforcement; f_{yt} is the specified yield strength of transverse reinforcement; and s is the center-to-center spacing of transverse reinforcement.

The contribution of FRCM to the nominal shear strength is calculated according to the following equation proposed by ACI 549 [15]:

$$V_f = nA_f f_{fv} d_f, \tag{3}$$

where n is the number of layers of mesh reinforcement; A_f is the area of mesh reinforcement by unit width; and d_f is the effective depth of the FRCM shear reinforcement.

The design tensile strength of the FRCM composite, f_{fv}, is calculated from the following:

$$f_{fv} = E_f \varepsilon_{fv}, \tag{4}$$

$$\varepsilon_{fv} = \varepsilon_{fu} \le 0.004, \tag{5}$$

where E_f, ε_{fv}, and ε_{fu} are the tensile modulus of elasticity of FRCM, the design tensile strain of FRCM shear reinforcement, and the ultimate tensile strain of FRCM, respectively.

The design tensile strain of the FRCM composite, ε_{fv}, is limited to 0.004 according to ACI 549 [15].

3.4.2. Proposed Equation. All beams strengthened with the hybrid FRP-FRCM in this study failed due to debonding of the FRCM composite. The debonding failure mode is governed by the bond strength between the concrete surface and the FRCM composite. Therefore, a prediction model of the contribution of the FRCM composite to the shear strength was proposed based on the bond strength between the concrete surface and the hybrid FRP-FRCM in this study. When the bond stress at the free end of FRCM reaches the ultimate bond stress, the distribution of the bond stress at the interface can be described as in Figure 11 [17].

The average bond stress of side-bonding and U-jacketing can be calculated from the following equations, respectively [22]:

$$\tau_{p.\text{Side-bonding}} = \frac{\int_{-h_f/2}^{h_f/2} \left(4\tau_{\mathrm{ult}}/h_f^2\right) x^2 dx}{h}, \tag{6}$$

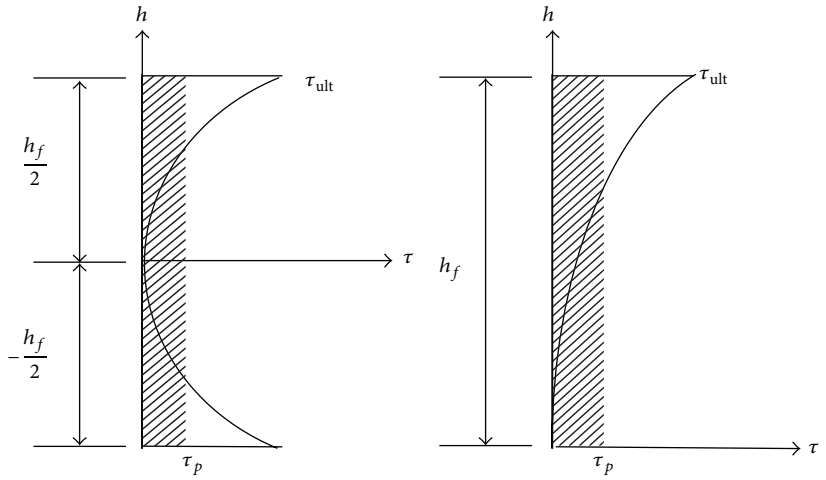

(a) Side-bonding type (b) U-jacketing type

Figure 11: Distribution of shear stress in each strengthening method [17].

$$\tau_{p.\text{U-jacketing}} = \frac{\int_0^{h_f} \left(\tau_{\text{ult}}/h_f^2\right) x^2 dx}{h}, \tag{7}$$

where h is the height of the beam, h_f is the height of the FRCM composite, τ_{ult} is the ultimate bond stress, and $\tau_{p.\text{Side-bonding}}$ and $\tau_{p.\text{U-jacketing}}$ are the average bond stress for side-bonding and U-jacketing, respectively.

Meanwhile, the average bond stress can be expressed as follows regardless of the FRCM bond type as the ultimate bond stress is the same:

$$\tau_p = \tau_{p.\text{Side-bonding}} = \tau_{p.\text{U-jacketing}}. \tag{8}$$

Therefore, the contribution of the hybrid FRP-FRCM to the nominal shear strength can be defined as follows:

$$V_f = 2T_f = 2\tau_p h_f \frac{w_f}{w} d\cot\theta, \tag{9}$$

where T_f is the bond strength of FRCM, d is the distance from the extreme compression fiber to the centroid of longitudinal tension reinforcement, θ is the inclination of the shear crack, w is the length of the shear span, and w_f is the width of the hybrid FRP fabric bonded on the shear span.

In (9), the average bond stress, τ_p, was determined from direct shear tests according to variation of the bond length, as shown in Figure 12. Bricks with dimensions of 100 mm × 100 mm × 200 mm were produced with concrete used in the beam manufacture process, and hybrid FRP-FRCM was bonded on both sides of the brick in the same manner as the beams were strengthened. The average bond stress according to the bond length was measured, and the test results are presented in Figure 13. The average bond stress tends to decrease with an increase of bond length until 140 mm and thereafter converges to 0.28 MPa. Therefore, the average shear stress, τ_p, was defined as 0.28 MPa in the proposed model. In addition, the inclination of the shear crack, θ, was defined as 45°. V_c and V_s were calculated by the ACI 318 code [21].

Figure 12: Setup of direct shear test.

3.4.3. Comparison between Experimental and Analytical Results. The shear strengths of FRCM shear strengthened beams predicted by ACI 549 [15] and the proposed model are tabulated in Table 6. Also, the ratios of the test results to the shear strengths predicted by ACI 549 [15] and the proposed model are presented in Table 6.

The ratios by ACI 549 [15] for specimens W600-L1 and W600-L2 strengthened by side-bonding were 0.98 and 0.69, respectively. It can be confirmed from these results that ACI 549 [15] overestimates the shear strength of FRCM shear strengthened beams by side-bonding and the prediction error increases with an increase of the amount of hybrid FRP. In contrast, the ratios by ACI 549 [15] for shear strengthened beams by U-jacketing ranged from 1.10 to 1.22. Namely, ACI 549 [15] underestimates the shear strength of shear strengthened beams by U-jacketing.

The ratios by the predicted model for specimens W600-L1 and W600-L2 strengthened by side-bonding were 0.88 and 0.94, respectively. Although the proposed model also

Table 6: Comparisons between predicted values and experimental results.

Specimen ID	P_{EXP} (kN)	ACI 549 [15]					Proposed model				
		V_c (kN)	V_s (kN)	V_{FRCM} (kN)	P_{ACI} (kN)	P_{EXP}/P_{ACI}	V_c (kN)	V_s (kN)	V_{FRCM} (kN)	$P_{Prop.}$ (kN)	$P_{EXP}/P_{Prop.}$
Control	105	36	—	—	72	1.46	36	—	—	72	1.46
S300	172		51	—	174	0.99		51	—	174	0.99
S200	168		77	—	226	0.74		77	—	226	0.74
W600-L1	143		—	37	146	0.98		—	45	162	0.88
W600-L2	152		—	74	220	0.69		—	45	162	0.94
W50-N4	117		—	12	96	1.22		—	15	102	1.15
W50-N5	123		—	15	102	1.21		—	19	110	1.12
W50-N6	127		—	19	110	1.15		—	23	118	1.08
W100-N3	121		—	19	110	1.10		—	23	118	1.03
W100-N4	144		—	25	122	1.18		—	30	132	1.09
W600-N1	162		—	37	146	1.11		—	45	162	1.00
Mean						1.08					1.04

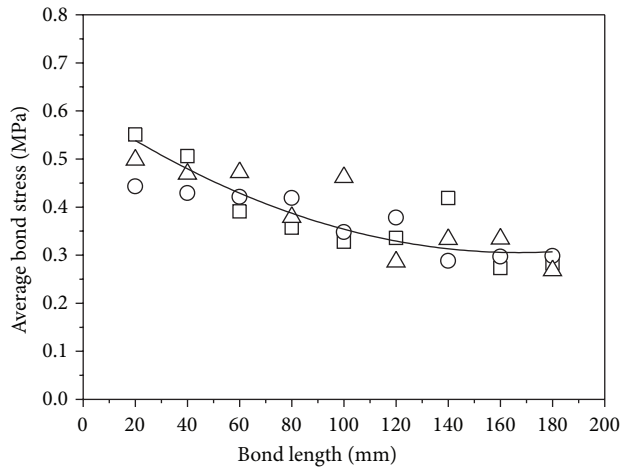

Figure 13: Average bond stress according to bond length.

overestimates the shear strength of the beams strengthened by side-bonding, the prediction error was smaller than that of the ACI 549 code [15]. Moreover, the ratios by the proposed model for the shear strengthened beams by U-jacketing ranged from 1.00 to 1.15, which are smaller than those given by the ACI 549 code [15]. This validates that the proposed model predicted the shear strength of beams strengthened by U-jacketing more reliably than ACI 549 [15] did.

3.4.4. Comparison between the Proposed Model and Existing Experimental Results. The performance of the proposed model was evaluated through a comparison between the numerically predicted values and existing experimental results [4, 10, 11, 14]. The geometry and material properties of RC beam specimens of the existing tests are presented in Table 7. Table 8 shows comparisons between the proposed model and existing experimental results. ACI 549 [15] requires the tensile modulus of elasticity for the FRCM, which is obtained from direct tensile test for the FRCM, to calculate the shear capacity of FRCM strengthened beams. However, the references in Table 7 did not present the tensile modulus of elasticity for the FRCM. Thus, the comparison between ACI 549 [15] and the existing experimental results has been excluded in the present study.

From Table 8, it can be confirmed that the proposed model predicts the existing experimental results well: the mean of the ratio between the proposed model and corresponding experimental results is 0.99 and its coefficient variable (COV) is 0.16. Accordingly, it can be concluded that the shear prediction model from this study could be widely used for shear capacity estimation of FRCM strengthened beams.

4. Conclusion

Conclusions obtained from this study are as follows.

(1) It was validated that the maximum load of shear strengthened beams with hybrid FRP-FRCM increased from 11.4% to 54.3% according to the amount of hybrid FRP, and the effectiveness of hybrid FRP for shear capacity is not proportional to the amount used.

(2) It was confirmed from test results that U-jacketing was more effective than side-bonding for FRCM shear strengthening.

(3) ACI 549 [15] overestimated the shear strength of beams strengthened by side-bonding with hybrid FRP-FRCM and the prediction error increases with an increase of the amount of hybrid FRP. In addition, ACI 549 [15] underestimated the shear strength of shear strengthened beams by U-jacketing.

(4) Although the proposed model also overestimated the shear strength of beams strengthened by side-bonding with hybrid FRP-FRCM, the prediction error was smaller than that of ACI 549 [15]. Moreover, for shear-strengthened beams by U-jacketing, the

Table 7: Geometry and material properties of RC beam specimens of experimental test database.

Reference	Specimen ID	b (mm)	d (mm)	h_f (mm)	f'_c (MPa)	A_v (mm^2)	f_{yt} (MPa)	s (mm)	w (mm)	w_f (mm)	a/d
[4]	SB-GT	150	307.5	350	37.5	—	—	—	1000	1000	3.25
	UW-GT	150	307.5	350	37.5	—	—	—	1000	1000	3.25
	SB-CT1	150	307.5	350	37.5	—	—	—	1000	1000	3.25
	UW-CT1	150	307.5	350	37.5	—	—	—	1000	1000	3.25
	SB-CT2	150	307.5	350	37.5	—	—	—	1000	1000	3.25
	UW-CT2	150	307.5	350	37.5	—	—	—	1000	1000	3.25
[10]	Beam 4	150	295	350	50.1	56.55	384	180	900	675	3.05
[11]	TRA1	150	225	250	30.76	100.53	446.06	292	675	675	3.00
	TRA2	150	225	250	30.76	100.53	446.06	260	675	345	3.00
	TRB1	150	225	250	45.02	100.53	442.25	210	625	625	2.78
	TRB2	150	225	250	29.16	100.53	442.25	210	625	625	2.78
	TRB3	150	225	250	29.16	100.53	442.25	210	625	295	2.78
	TRB4	150	225	250	38.26	100.53	442.25	210	625	295	2.78
	TRB5	150	225	250	38.26	100.53	442.25	210	625	295	2.78
[14]	BS2	150	175	200	20	—	—	—	400	400	2.29
	BS3	150	175	200	20	—	—	—	400	400	2.29
	BS4	150	175	200	20	—	—	—	400	400	2.29
	BS5	150	175	200	20	—	—	—	400	400	2.29

Table 8: Comparisons between the existing experimental results and proposed model.

Reference	Specimen ID	Type of bond	Type of fiber	ρ_f (%)	P_{Exp} (kN)	V_c (kN)	V_s (kN)	V_{FRCM} (kN)	$P_{\text{Prop.}}$ (kN)	$P_{\text{Exp}}/P_{\text{Prop.}}$
[4]	SB-GT	S	G	0.297	146.3	48.02	—	60.27	216.6	0.68
	UW-GT	U	G	0.297	180.2	48.02	—	60.27	216.6	0.83
	SB-CT1	S	C	0.229	155.5	48.02	—	60.27	216.6	0.72
	UW-CT1	U	C	0.229	151.8	48.02	—	60.27	216.6	0.70
	SB-CT2	S	C	0.516	245.4	48.02	—	60.27	216.6	1.13
	UW-CT2	U	C	0.516	253.4	48.02	—	60.27	216.6	1.17
[10]	Beam 4	U	G	0.096	294.0	53.25	35.59	43.37	264.4	1.11
[11]	TRA1	S	P	0.135	188.7	31.82	34.55	31.47	195.7	0.96
	TRA2	U	P	0.034	170.4	31.82	38.81	16.10	173.5	0.98
	TRB1	S	P	0.202	279.1	31.82	38.81	47.02	235.3	1.19
	TRB2	S	P	0.202	191.7	31.82	38.81	39.47	220.2	0.87
	TRB3	U	P	0.095	191.9	31.82	38.81	22.87	187.0	1.03
	TRB4	U	P	0.095	200.0	31.82	38.81	27.37	196.0	1.02
	TRB5	U	P	0.095	199.8	31.82	38.81	27.37	196.0	1.02
[14]	BS2	S	B	0.195	82.7	19.96	—	19.6	79.1	1.05
	BS3	S	B	0.195	83.5	19.96	—	19.6	79.1	1.06
	BS4	S	B	0.390	88.7	19.96	—	19.6	79.1	1.12
	BS5	S	B	0.390	92.5	19.96	—	19.6	79.1	1.17
Mean										0.99
Coefficient of variation										0.16

Note. S = side-bonding; U = U-jacketing; G = glass; C = carbon; P = PBO; B = basalt.

proposed model predicted the shear strength more reliably than ACI 549 [15] did.

(5) The agreement between the proposed model and the existing experimental results was very good. Accordingly, it can be concluded that the shear prediction model from this study could be widely used for shear capacity estimation of FRCM strengthened beams.

Conflict of Interests

The authors declare that there is no conflict of interests regarding the publication of this paper.

Acknowledgment

This work (Grant no. C0135751) was supported by Business for Cooperative R&D between Industry, Academy, and Research Institute funded by Korea Small and Medium Business Administration in 2013.

References

[1] L. C. Hollaway and M. B. Leeming, *Strengthening of Reinforced Concrete Structures Using Externally-Bonded FRP Composites in Structural and Civil Engineering*, Woodhead Publishing, Cambridge, UK, 1999.

[2] A. D'Ambrisi and F. Focacci, "Flexural strengthening of RC beams with cement-based composites," *Journal of Composites for Construction*, vol. 15, no. 5, pp. 707–720, 2011.

[3] G. Loreto, L. Leardini, D. Arboleda, and A. Nanni, "Performance of RC slab-type elements strengthened with fabric-reinforced cementitious-matrix composites," *Journal of Composites for Construction*, vol. 18, no. 3, Article ID A4013003, 2014.

[4] R. Azam and K. Soudki, "FRCM strengthening of shear-critical RC beams," *Journal of Composites for Construction*, vol. 18, no. 5, 2014.

[5] S. Babaeidarabad, G. Loreto, and A. Nanni, "Flexural strengthening of RC beams with an externally bonded fabric-reinforced cementitious matrix," *Journal of Composites for Construction*, vol. 18, no. 5, 2014.

[6] W. Brameshuber, T. Brockmann, M. Curbach et al., "State of the art report 36: textile reinforced concrete," RILEM TC 201-TRC, RILEM, 2006.

[7] T. C. Triantafillou and C. G. Papanicolaou, "Shear strengthening of reinforced concrete members with textile reinforced mortar (TRM) jackets," *Materials and Structures*, vol. 39, no. 285, pp. 93–103, 2006.

[8] H. C. Wu and P. Sun, "Fiber reinforced cement based composite sheets for structural retrofit," in *Proceedings of the International Symposium in Bond Behaviour of FRP in Structures (BBFS '05)*, pp. 351–356, International Institute for FRP in Construction, Hong Kong, China, 2005.

[9] T. Blanksvärd, B. Täljsten, and A. Carolin, "Shear strengthening of concrete structures with the use of mineral-based composites," *Journal of Composites for Construction*, vol. 13, no. 1, pp. 25–34, 2009.

[10] D. Baggio, K. Soudki, and M. Noël, "Strengthening of shear critical RC beams with various FRP systems," *Construction and Building Materials*, vol. 66, pp. 634–644, 2014.

[11] L. Ombres, "Structural performances of reinforced concrete beams strengthened in shear with a cement based fiber composite material," *Composite Structures*, vol. 122, pp. 316–329, 2015.

[12] A. Brückner, R. Ortlepp, and M. Curbach, "Anchoring of shear strengthening for T-beams made of textile reinforced concrete (TRC)," *Materials and Structures*, vol. 41, no. 2, pp. 407–418, 2008.

[13] A. Brückner, R. Ortlepp, and M. Curbach, "Textile reinforced concrete for strengthening in bending and shear," *Materials and Structures*, vol. 39, no. 292, pp. 741–748, 2006.

[14] Y. A. Al-Salloum, H. M. Elsanadedy, S. H. Alsayed, and R. A. Iqbal, "Experimental and numerical study for the shear strengthening of reinforced concrete beams using textile-reinforced mortar," *Journal of Composites for Construction*, vol. 16, no. 1, pp. 74–90, 2012.

[15] American Concrete Institute (ACI), "Design and construction guide of externally bonded FRCM systems for concrete and masonry repair and strengthening," ACI 549, American Concrete Institute, Farmington Hills, Mich, USA, 2013.

[16] ICC Evaluation Service, "Acceptance criteria for masonry and concrete strengthening using fiber reinforced cementitious matrix (FRCM) composite systems," Tech. Rep. AC434, ICC Evaluation Service, Whittier, Calif, USA, 2013.

[17] G. J. Al-Sulaimani, A. Sharif, I. A. Basunbul, M. H. Baluch, and B. N. Ghaleb, "Shear repair for reinforced concrete by fiberglass plate bonding," *ACI Structural Journal*, vol. 91, no. 4, pp. 458–464, 1994.

[18] ASTM International, "Standard test method for compressive strength of cylindrical concrete specimens," Tech. Rep. C39/C39M, ASTM International, West Conshohocken, Pa, USA, 2013.

[19] ASTM, "Standard test methods and definitions for mechanical testing of steel products," A370, ASTM, West Conshohocken, Pa, USA, 2013.

[20] ASTM, "Standard test method for compressive strength of hydraulic cement mortars," ASTM C109/C109M, ASTM, West Conshohocken, Pa, USA, 2013.

[21] American Concrete Institute (ACI), "Building code requirements for reinforced concrete," ACI 318, American Concrete Institute, Farmington Hills, Mich, USA, 2011.

[22] J. S. Sim, H. S. Oh, and J. M. Yu, "A study on the prediction model of shear strength of RC beams strengthened for shear by FRP," *Journal of the Korea Concrete Institute*, vol. 12, no. 5, pp. 35–46, 2000 (Korean).